hydrology

MDPI

Article

A Singh-Based Fuzzy Logic Framework for Short-Term Discharge and Flood Peak Prediction Under Data-Scarce Hydrological Conditions

Mahshid Khazaeiathar * and Britta Schmalz

Engineering Hydrology and Water Management (ihwb), Technical University of Darmstadt, 64287 Darmstadt, Germany; b.schmalz@ihwb.tu-darmstadt.de
* Correspondence: m.khazaei@ihwb.tu-darmstadt.de

Abstract

Short-term discharge forecasting remains challenging under highly variable, nonlinear, and data-constrained hydrological conditions, where conventional machine learning and deep learning approaches require large datasets and extensive parameterisation, and offer limited interpretability. This study proposes a Singh-based fuzzy logic framework for one-hour-ahead discharge and flood peak prediction using hourly streamflow from the Schwarzbach catchment (135 km^2, Hesse, Germany). Four storm-driven flood events were analysed under contrasting hydrological conditions. Temporal dependence was characterised using autocorrelation function (ACF), partial autocorrelation function (PACF), and fuzzy-cluster transition analysis to link event-specific discharge dynamics with predictive behaviour. The results revealed substantial heterogeneity in hydrological memory, autocorrelation decay, and state-transition complexity across events, ranging from smooth memory-dominated responses to oscillatory multi-peak behaviour. Despite these differences, the framework reproduced all flood events with Nash–Sutcliffe efficiency (NSE) above 0.99 while capturing peak timing and magnitude, including complex double-peak dynamics. Because NSE is referenced to the variance of the observed series, forecasts were benchmarked against a persistence predictor, which itself attains a NSE of 0.958–0.976 at this lead time and time step; relative to persistence the framework reduced the root mean squared error by 38–68%, corresponding to skill scores of 0.612–0.897, whereas an AR(1) benchmark yielded no meaningful improvement. Prediction uncertainty increased with hydrological complexity but remained free of systematic bias. The results demonstrate that fuzzy logic provides an interpretable and computationally efficient alternative for short-term discharge forecasting that improves measurably on a naïve benchmark, offering potential for flood early warning systems and water resource management in data-scarce catchments.

Keywords: fuzzy logic; discharge; singh method; short-term; flood peak; modelling; data-scarce; one-hour-ahead forecasting; persistence benchmark; skill score

Check for updates

Academic Editor: Salvatore Manfreda

Received: 15 July 2026
Revised: 1 September 2026
Accepted: 3 September 2026
Published: 7 September 2026

Copyright: © 2026 by the authors. Licensee MDPI, Basel, Switzerland. This article is an open access article distributed under the terms and conditions of the Creative Commons Attribution (CC BY) license.

1. Introduction

According to the report published by the Centre for Research on the Epidemiology of Disasters and United Nations Office for Disaster Risk Reduction (CRED and UNDRR) [1] in 2020, climate-related hazards such as extreme precipitation and floods have increasingly dominated natural disasters in recent decades. As the frequency and magnitude of these events continue to rise, accurate and timely flood forecasting (FF) has become essential for enhancing disaster resilience. In particular, short-term FF (from hours to days before

an event) can be effectively incorporated into flood early warning frameworks to support timely response and risk reduction [2,3]. Accordingly, this study adopts a one-hour-ahead (one-step) forecasting horizon on hourly discharge, a lead time consistent with the rapid storm-driven response of the small (135 km^2) Schwarzbach catchment, and therefore is operationally relevant for local early warning.

Flood forecasting approaches can generally be classified into physically based, stochastic, machine learning-based, and hybrid methods. Among these, physically based models describe hydrological processes using mathematical formulations of watershed and flow dynamics. Representative examples of physically based hydrological models include WASH123D [4], HEC-HMS [5], SWMM [6], and SWAT [7]. These models have been successfully applied to simulate rainfall–runoff and flood processes [8,9]. However, physically based models are associated with two major limitations: (a) the need for detailed information about the catchment [10], and (b) high model complexity, which may restrict their applicability and transferability to other regions [11].

Stochastic models incorporate uncertainty and randomness into their mathematical structure, enabling a more flexible representation of hydrological processes [12]. In flood forecasting applications, these models can generate multiple possible scenarios and capture underlying temporal patterns using historical observations [2,13]. Commonly used stochastic approaches include autoregressive moving average models [14], and Monte Carlo simulation methods [15].

Machine learning models are designed to emulate human cognitive capabilities by identifying complex patterns and relationships within datasets through adaptive computational algorithms [16]. In recent years, these approaches have demonstrated remarkable capability in hydrological applications. For instance, artificial neural networks (ANNs), composed of interconnected computational units, have been successfully utilised to predict floods by learning nonlinear relationships from historical observations [17]. ANNs face notable limitations in forecasting tasks [18], driving growing interest in deep learning (DL) models. These architectures utilise multiple layers of interconnected nodes, enabling the extraction of complex patterns from data. DL offers two key advantages: rapid output generation [19] and high predictive accuracy. Indeed, DL-based approaches have in some cases outperformed conventional physically and stochastically based flood forecasting methods [20]. Despite these strengths, however, DL models suffer from a black-box nature, limiting the interpretability of their decision-making processes. This has consequently prompted the emergence of explainable AI (XAI) techniques as a means of enhancing model transparency [21].

To address the limitations of individual forecasting approaches, recent research has increasingly focused on hybrid frameworks that integrate the advantages of multiple modelling techniques [22,23]. Incorporating hydrological knowledge and process-based understanding into forecasting models can improve both physical consistency and model interpretability [24,25]. In this context, Fuzzy Logic-based models have gained considerable attention due to their ability to represent uncertainty, nonlinear hydrological behaviour, and imprecise relationships inherent in flood forecasting systems. Owing to their transparent rule-based structure and flexible inference mechanism, these models can improve forecasting performance while providing more reliable and interpretable short-term flood predictions. For instance, Alvisi et al. [26] compared Mamdani and Takagi–Sugeno Fuzzy Logic models with ANN models for water level forecasting using rainfall and river water level data from the Reno River, Italy. Their findings indicated that Fuzzy Logic approaches achieved better forecasting performance when hydrological processes were represented through a limited number of variables and IF–THEN rule-based relationships. In addition, Wee et al. [27] developed a Fuzzy Logic-based flood impact forecasting system for the Ke-

maman River basin in Malaysia by integrating hazard, exposure, and vulnerability factors within a multi-layer fuzzy inference framework. Their results showed that the proposed Fuzzy Logic approach effectively captured complex flood interactions and provided reliable short-term flood warning information for risk reduction and decision support.

Despite these advances, limited attention has been given to interpretable Fuzzy Logic frameworks specifically designed for short-term discharge prediction under highly variable and data-constrained hydrological conditions. Nevertheless, many existing ML- and DL-based flood forecasting approaches depend on large training datasets, extensive parameterisation, and computationally demanding architectures. These characteristics limit their applicability for short-term hydrological prediction under data-scarce and highly volatile conditions. Moreover, the black-box nature of these models often constrains physical interpretability and reduces their practical reliability in flood early warning and decision-support applications. Hydrological systems are inherently governed by nonlinear interactions, uncertainty, spatial–temporal variability, and imprecise process boundaries. These complexities become even more critical during rapidly evolving flood events, where discharge dynamics can change abruptly over short time scales. Under such conditions, purely data-driven approaches may struggle to preserve stable, transparent, and physically meaningful predictive behaviour.

To address these challenges, this study proposes a Fuzzy Logic framework for short-term discharge and flood peak prediction using hourly streamflow observations. Unlike conventional black-box models, the proposed framework utilises fuzzy membership functions and statistical behaviour-based clustering to represent nonlinear, uncertain, and complex temporally dependent discharge dynamics without relying on restrictive distributional assumptions. In addition, the model avoids extensive parameter estimation procedures that commonly complicate conventional hydrological modelling approaches.

These characteristics make Fuzzy Logic particularly suitable for modelling short-term discharge series, where limited observations, complex temporal dependence, and uncertainty frequently dominate the system response. Furthermore, the proposed framework aims to enhance peak-flow representation while maintaining low computational complexity, transparent reasoning mechanisms, and stable predictive behaviour under uncertain hydrological conditions. Therefore, the findings of this study can contribute to the development of more reliable flood early warning systems, adaptive flood risk management strategies, and resilient water resource decision-making frameworks. The specific contributions of this study are (1) the first application of a Singh-based fuzzy partitioning scheme to short-term streamflow forecasting under data-scarce and highly variable hydrological conditions; (2) a combined ACF–PACF–cluster-transition diagnostic framework that explicitly links the temporal dependence structure of each flood event to its predictive performance, providing mechanistic transparency absent in black-box approaches; and (3) demonstration of robust flood peak reproduction—including complex double-peak dynamics, achieved from minimal training data (5–6 days per event), establishing the practical viability of the framework for operational early warning in data-limited catchments.

This paper is divided as follows: Section 2 contains the study area and data description, methods are discussed in Section 3, results and discussion are presented in Section 4, and finally, Section 5 shows the conclusion.

2. Study Area and Data Description

This study targets the Schwarzbach river catchment upstream of the Nauheim gauge (ID: 23980353; 49.9508° N, 8.4526° E [28]), located in Groß-Gerau district, Hesse, Germany. With a total drainage area of 135 km^2 [28], the catchment belongs to the Rhine River Basin district and simultaneously serves as a test site for the LOEWE Research Centre emer-

genCITY (https://www.emergencity.de (accessed on 5 February 2026)). This work was conducted within the sub-project "Smart Flood and Low-Flow Warning System" of the emergenCITY initiative, which aims to strengthen the resilience of smart-city infrastructures against natural disasters. The sub-project focuses on developing an environmental monitoring and warning system for the early assessment and forecasting of floods and low-flow events by integrating real-time measurement data from multiple sources through artificial intelligence-based data fusion techniques.

Topographically, the area is flat, forming part of the Rhine River Plain. Agriculture dominates land cover, though sizeable settlements; Mörfelden-Walldorf, Langen, and Nauheim; punctuate the landscape. Frankfurt International Airport, the largest in Germany, occupies the northern catchment boundary. Two tributaries, the Gundbach and Geräthsbach, merge to form the Schwarzbach, which then runs south-westward until cutting through the centre of Nauheim at the gauge location. The catchment area and the location of the Nauheim gauge are presented in Figure 1.

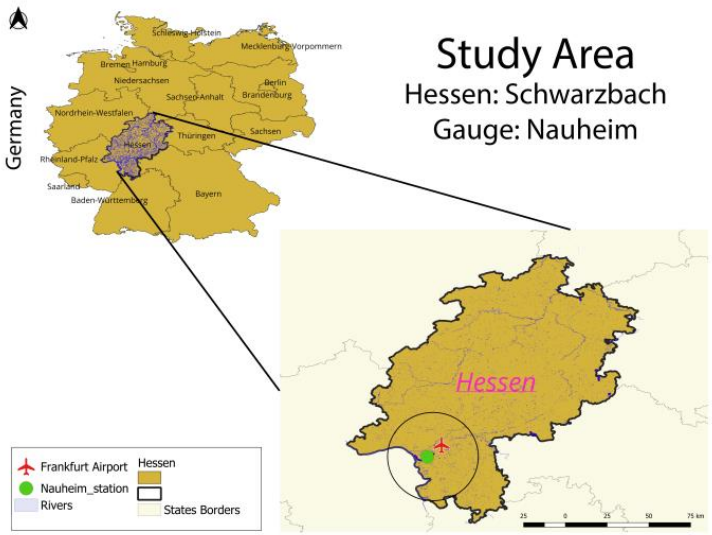


Figure 1. Schwarzbach Catchment, Nauheim Gauge (HLNUG 2026 [28]).

Discharge statistics compiled over 1965–2009 place the mean flow at 0.60 m^3/s, while the lowest and highest recorded values reached 0.02 m^3/s (28 August 1976) and 5.00 m^3/s (11 June 1965), respectively [29]. The dataset covers four storm-driven flood events. Events were identified from the 10 min precipitation series of DWD station Frankfurt/Main Flughafen (ID 1420). The selection threshold was a cumulative event precipitation depth of at least 25 mm. In addition, the four events occurred in separate years. Accordingly, they are hydrologically independent:

- E1: 8–14 June 2013
- E2: 15–20 August 2012
- E3: 20–26 July 2004
- E4: 1–7 May 2000

River discharge was recorded every 15 min across 1985–2023 [30], complemented by 10 min precipitation observations from DWD station Frankfurt/M for 1993–2023 (data source: [31], Flughafen (ID 1420)). The full 39-year discharge record was not used for modelling. Instead, only the four event windows defined above were extracted. Each window therefore provides 5–6 days of hourly discharge as model input. Tables 1 and 2 summarise the statistical characteristics of the discharge and precipitation time series for each event, respectively. Figure 2 presents the corresponding precipitation hyetographs and discharge hydrographs for the four selected flood events.

Table 1. Statistical Characteristics of Discharge Time Series for Events 1–4.

Event	Mean (m^3/s)	SD (m^3/s)	Variance $(m^3/s)^2$	Max (m^3/s)	Min (m^3/s)	CV
Event 1	0.9612	0.3243	0.1052	1.83	0.59	0.3374
Event 2	0.5929	0.484	0.2343	1.78	0.143	0.8164
Event 3	0.3892	0.2778	0.0772	1.18	0.195	0.7138
Event 4	1.0157	0.3887	0.1511	1.76	0.41	0.3827

SD: Standard Deviation; CV: Coefficient of Variation.

Table 2. Statistical Characteristics of Precipitation Time Series for Events 1–4.

Event	Mean (mm)	SD (mm)	Variance $(mm)^2$	Max (mm)	Min (mm)	CV
Event 1	0.0671	0.7442	0.5532	18.39	0	11.08
Event 2	0.0698	0.7086	0.5021	12.91	0	10.14
Event 3	0.0506	0.8591	0.7381	19.5	0	16.94
Event 4	0.0663	0.6926	0.4797	14	0	10.44

SD: Standard Deviation; CV: Coefficient of Variation.

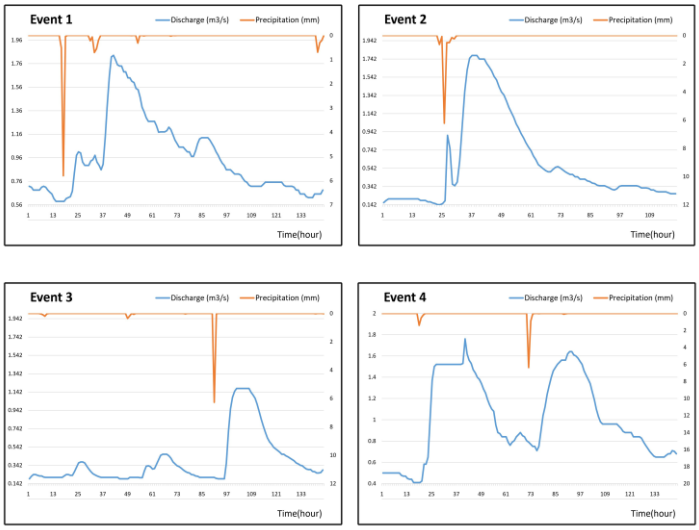


Figure 2. Discharge hydrographs (First y-axes) and precipitation hyetographs (second y-axes) for the four selected flood events.

Event 4 recorded the highest mean discharge (1.016 m^3/s), while Event 3 had the lowest mean (0.389 m^3/s) and the smallest peak (1.18 m^3/s). Despite comparable peak discharges across Events 1–4 (ranging from 1.18 to 1.83 m^3/s), Event 2 exhibited the greatest internal variability (CV = 0.817), reflecting its steep rise and rapid recession, whereas Event 1 showed the most stable discharge evolution (CV = 0.337), consistent with its prolonged, oscillatory hydrograph shape.

3. Methods

In this study, the term data-scarce refers to situations where the available observations are insufficient to train data-intensive machine learning or deep learning models reliably, regardless of whether this limitation arises from short observation periods, few recorded events, or other practical data constraints. Consequently, the proposed fuzzy-logic framework is designed as an alternative forecasting approach for such limited-data conditions.

Importantly, data scarcity here is imposed by design rather than encountered in the catchment: the framework is applied to four event windows of only 5–6 days of hourly discharge each. The Schwarzbach was selected for precisely this reason. Its long and reliable record permits a controlled test, because the model operates on an event-scale subset while an independent long-term record remains available in the catchment, which would not be the case in a genuinely ungauged basin.

To facilitate the application of the fuzzy-logic framework, the original 15 min streamflow records were resampled to an hourly temporal resolution by averaging every four consecutive observations. This aggregation step serves multiple methodological purposes. First, high-frequency hydrological time series commonly exhibit short-term noise and measurement irregularities that do not reflect actual hydrological dynamics [32]; averaging suppresses these artefacts and yields a smoother, more physically representative signal. Second, reducing the sampling frequency decreases data dimensionality, which in turn lowers computational overhead and improves the tractability of the modelling procedure. Third, and most critically for the fuzzy-logic context, fuzzy inference systems rely on membership functions whose boundaries must be stably estimated from the input data distribution [33,34]. High-frequency fluctuations inflate local variance and can distort membership function shapes, leading to poorly defined rule-based relationships and reduced generalisation performance [35]. Hourly aggregation effectively narrows this variance, producing a more stable and well-conditioned input signal that is better suited to fuzzy partitioning. Following this preprocessing step, a systematic procedure was developed to assess model suitability and construct the fuzzy logic forecasting framework. It should be noted that this temporal aggregation was performed solely as a preprocessing step to support the development of the proposed hourly forecasting framework. The overall workflow is illustrated in Figure 3.

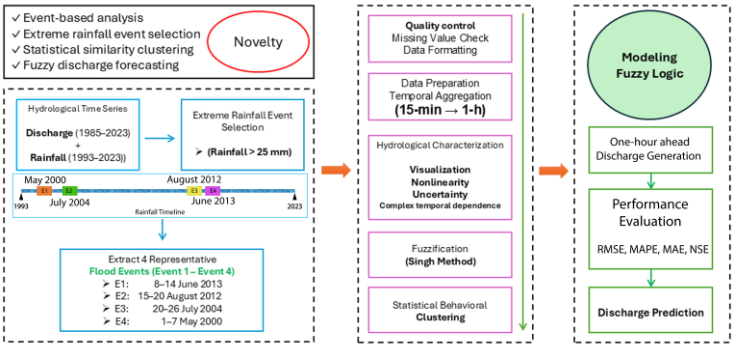


Figure 3. Flowchart of the proposed methodology for discharge forecasting.

3.1. Autocorrelation Function (ACF)

The ACF was employed as a multi-purpose diagnostic tool to characterise three key properties of the observed discharge series: nonlinearity, uncertainty, and complex temporal dependence. These properties collectively motivate the adoption of the Singh fuzzy logic framework.

3.1.1. Nonlinearity

Nonlinearity in a hydrological time series implies that the relationship between past and future discharge values cannot be adequately described by a linear model [36]. To assess this property, the ACF was applied to the hourly discharge series. The ACF quantifies the correlation between an observation and its lagged counterparts across a range of time intervals [37–39], enabling the detection of asymmetric decay patterns, oscillatory structures, and irregular persistence horizons that are symptomatic of nonlinear dynamics [40].

Departures from a smooth, exponential ACF decay, such as non-monotonic decline or sign alternation, provide evidence that the underlying process involves nonlinear interactions among discharge states [41]. The ACF at lag τ is expressed as:

$$r_k = \frac{\sum_{t=1}^{N-K}(x_t - x^-)(x_{t+k} - x^-)}{\sum_{t=1}^{N}(x_t - x^-)^2} \quad (1)$$

where r_k denotes the sample autocorrelation at lag K; x_t and x_{t+k} represent the signal values at times t and $t + k$, respectively; x^- is the sample mean; and N is the total integration duration.

3.1.2. Uncertainty

Beyond nonlinearity detection, the ACF was also applied to quantify uncertainty in the temporal dependence structure of the discharge series. Uncertainty in this context refers to the variability and unpredictability of autocorrelation patterns across different events and time windows [2,41]. When ACF profiles differ substantially across flood events, in terms of decay rate, persistence horizon, or oscillatory character, this event-to-event variability reflects an inherently uncertain dependence structure that resists characterisation by a fixed parametric model [42]. Such variability implies that no single correlation function can reliably represent the full range of observed dynamics [43]. The magnitude and structure of this uncertainty cannot be bounded by conventional confidence intervals alone, as the source of variability lies in the process itself rather than in estimation error [44,45]. The mathematical formulation of the ACF applied in this assessment is provided in Equation (1) of Section 3.1.1.

3.1.3. Complex Temporal Dependence

The ACF was further examined to assess the complexity of temporal dependence in the discharge series. Complex temporal dependence arises when the correlation structure of a time series cannot be described by a single time scale or a uniform decay pattern [45,46]. In hydrological systems, such complexity emerges from the superposition of multiple physical mechanisms—including surface runoff, baseflow contributions, and antecedent soil moisture effects—that operate simultaneously at different temporal scales [47]. When the ACF exhibits multiple persistence horizons, oscillatory structures, or abrupt transitions in correlation decay, these features indicate that the dependence structure is governed by several interacting processes rather than a single dominant one [2,41]. The presence of such multi-scale dependence renders conventional single-order linear models inadequate and motivates the use of flexible inference frameworks capable of representing heterogeneous temporal relationships.

3.2. Partial Autocorrelation Function (PACF)

Complementary to the ACF, the PACF was employed to further characterise the discharge series with respect to nonlinearity, uncertainty, and complex temporal dependence. The PACF isolates the direct linear relationship between an observation and its lagged value at a specific lag [45,46], by removing the influence of all intermediate lags between the two time points under consideration [47]. This property makes the PACF particularly informative for identifying genuine lag-specific dependencies and distinguishing them from indirect propagation effects.

3.2.1. Nonlinearity

In the context of nonlinearity assessment, the PACF provides complementary evidence to the ACF. It reveals whether the direct dependencies between discharge observations

at specific lags deviate from the patterns expected under a linear autoregressive structure [36,45]. Nonlinearity manifests in the PACF as irregular spike patterns, alternating sign sequences, or the simultaneous significance of multiple non-adjacent lags [39,46]. Such features indicate that the discharge process involves direct nonlinear interactions that cannot be captured by a single linear autoregressive model [48]. These characteristics were assessed alongside the ACF to evaluate the nonlinear properties of the hourly discharge series. The PACF at lag k is defined as:

$$X_t = c + \varphi_{k_1} x_{t-1} + \varphi_{k_2} X_{t-2} + \ldots + \varphi_{k_k} X_{t-k} + \in_t \quad (2)$$

where X_t denotes the discharge value at time t; φ_{k_1}, φ_{k_2}, ..., φ_{k_k} are the autoregressive coefficients estimated from an $AR(K)$ model; φ_{k_k} corresponds to the partial autocorrelation coefficient at lag k; and ϵ_t is a white-noise error term.

3.2.2. Uncertainty

For uncertainty assessment, the PACF was examined to detect variability in direct lag dependencies across the four flood events [49]. Uncertainty in the PACF context refers to the inconsistency of partial autocorrelation profiles across events—manifesting as event-specific significant lags that shift in position, magnitude, and sign [50]. When no stable set of significant partial autocorrelations can be identified across events, the direct dependence structure is considered uncertain and resistant to fixed-order parametric modelling [51,52]. These patterns were evaluated in conjunction with the ACF results to provide a comprehensive characterisation of the discharge series prior to fuzzy logic model development.

3.2.3. Complex Temporal Dependence

The PACF was additionally examined to characterise the complexity of direct temporal dependence in the discharge series. Complex temporal dependence in the PACF sense refers to the simultaneous significance of multiple non-adjacent lags or the co-occurrence of competing positive and negative partial autocorrelations at higher lag orders [36,45]. Such patterns indicate that the discharge process is driven by several direct influences operating at distinct temporal scales, rather than a single dominant autoregressive component [39,46]. The event-specific nature of these multi-lag interactions further underscores the heterogeneity and complexity of the underlying hydrological dynamics [49,51]. Together, the PACF evidence for nonlinearity, uncertainty, and complex temporal dependence corroborates the ACF findings and reinforces the rationale for employing the Singh fuzzy logic framework, which accommodates heterogeneous and multi-scale direct dependencies through adaptive rule-based inference.

3.3. Fuzzification (Singh Method)

Fuzzification, the foundational stage of any fuzzy time series framework [53], maps crisp observations onto linguistic fuzzy sets defined over a universe of discourse [54]. The hourly discharge series was fuzzified using the computational scheme of Singh [55], chosen for (a) its low computational complexity [56]; (b) its avoidance of cumbersome fuzzy relational matrix operations [57]; and (c) its robustness in modelling nonlinear, uncertain hydrological dynamics [58,59].

The universe of discourse U, which bounds the range of admissible discharge values, was first defined as:

$$U = [D_{min} - \delta_1, D_{max} + \delta_2] \quad (3)$$

where D_{min} and D_{max} are the minimum and maximum observed discharge values, and δ_1 and δ_2 are positive scalars that extend the bounds so that extreme flood peaks near the data limits remain represented.

The universe was partitioned into intervals u_1, ..., u_m, each supporting a fuzzy set A_i. Using triangular membership functions, the membership of an observation D in A_i was computed as:

$$\mu_{A_i}(D) = max\left(\left(0, min\left(\frac{(D - a_i)}{(b_i - a_i)}\right), \frac{(c_i - D)}{(c_i - b_i)}\right)\right) \quad (4)$$

where a_i, b_i, and c_i are the lower bound, peak, and upper bound of A_i, and $\mu_{A_i}(D) \in [0, 1]$ is the membership grade. Each observation was assigned to the fuzzy set of highest membership, yielding the fuzzified series.

Distinctively, the Singh scheme derives the interval length from the data rather than fixing it arbitrarily, important for discharge series with a wide low-flow-to-peak range [60]. The interval length L was set from the mean absolute first-order difference of the series:

$$L = (1/2).(1/(N-1)).\sum_{t=1}^{N}|D_t - D_{t-1}| \quad (5)$$

where D_t and D_{t-1} are consecutive observations, N is the number of observations, and the factor 1/2 scales the mean difference to a representative interval width. Rather than a full relational matrix, the Singh method uses the differences between successive fuzzified states as the forecasting parameter—the source of its linear-order efficiency. This representation preserves the gradual transitions characteristic of hydrological processes and provides the basis for the fuzzy logical relationships built in the next stage [61].

In this study, the number of intervals was set to n = 8. This selection reflects a critical modelling decision in fuzzy time series forecasting, as it directly governs the granularity of the fuzzification and the completeness of the resulting rule base [60]. Huarng [62] demonstrated that interval length significantly influences forecasting accuracy. Specifically, too few intervals cause excessive information loss, whereas too many intervals lead to sparsely populated rule groups [60,63]. Chen [54] adopted seven equal intervals as a widely cited baseline partition, which has since been applied and extended in numerous studies. The broader fuzzy time series literature reports that optimal interval counts typically range from 7 to 13, depending on data range, distribution, and the degree of variability in the series [60,64].

For the hourly discharge series under study, which spans a wide low-flow-to-peak range with high short-term variability, n = 8 intervals was selected as a parsimonious yet informative partition: it provides one additional interval beyond Chen's baseline to accommodate the discharge dynamics more precisely, while keeping computational cost minimal and the fuzzy rule base sufficiently dense for reliable inference. As a first-order fuzzy time series model, the Singh scheme forecasts the state at t + 1 from the difference between successive fuzzified states, so that the forecasting horizon corresponds to a single time step, i.e., one hour ahead for the hourly discharge series analysed here. All forecasts and performance metrics reported in this study therefore refer to this one-hour-ahead horizon; longer horizons would require recursive iteration or a high-order formulation, which were not applied. The proposed fuzzy time series model was implemented independently for each of the four flood events using the corresponding hourly discharge record. For each event, the model generated a one-hour-ahead discharge series over the event duration. Model performance was subsequently evaluated by comparing the generated and observed discharge series using RMSE, MAE, MAPE, and NSE. The evaluation was performed separately for each event to assess the capability of the proposed framework to reproduce the temporal evolution of the observed flood hydrograph.

Finally, the bounds of the universe of discourse in Equation (3) and the interval length in Equation (5) are derived from the complete event window, including its maximum. These are not calibrated parameters, and no training/testing partition is therefore involved; they do, however, require the range of the event to be known in advance. In a real-time

application the event maximum is not available, so the configuration reported here is not directly reproducible in operational forecasting. For the present dataset this effect is not negligible: the interval length L estimated from the first 24 h of each event differs from the full-window value by up to a factor of eight (Event 2: L = 0.0023 m^3/s versus 0.0192 m^3/s), because the early low-flow period contains far smaller successive differences than the flood limbs. An operational implementation would therefore require U and L to be fixed a priori from an independent historical record, or to be updated recursively as the event unfolds. The results presented here should accordingly be understood as a controlled assessment of the predictive capability of the Singh partitioning scheme rather than as a demonstration of a deployed real-time system.

3.4. Evaluation Metrics

3.4.1. Root Mean Squared Error (RMSE)

RMSE quantifies the typical magnitude of discrepancy between predicted and observed discharge values, expressed in the same physical units as the variable of interest [65]. Because errors are squared prior to averaging, RMSE penalises larger deviations more heavily than smaller ones, making it particularly sensitive to peak-flow errors; lower values indicate superior model performance [66]. RMSE is defined as:

$$RMSE = \sqrt{\frac{\sum_{i=1}^{N}(y_i - \hat{y_i})^2}{N}} \quad (6)$$

where y_i and $\hat{y_i}$ denote the observed and predicted values at time step i, respectively, and N is the total number of data points.

3.4.2. Mean Absolute Percentage Error (MAPE)

MAPE expresses the average relative deviation of simulated from observed discharges as a percentage, rendering it independent of the measurement scale [67]. This scale invariance facilitates straightforward comparisons across catchments or forecasting lead times, and smaller MAPE values correspond to higher forecasting skill [68]. The metric is computed as:

$$MAPE = \frac{100}{N}\sum_{i=1}^{N}\left|\frac{y_i - \hat{y_i}}{y_i}\right| \quad (7)$$

where y_i is the observed discharge, $\hat{y_i}$ is the model-predicted discharge, and N is the number of observations.

3.4.3. Mean Absolute Error (MAE)

MAE measures the average absolute discrepancy between simulated and observed discharge, assigning equal weight to all individual errors regardless of their sign or magnitude [69]. Its linear character makes it more robust to outliers than squared-error metrics, while retaining direct interpretability in the original data units. As with RMSE, smaller values reflect better predictive accuracy [68]. MAE is expressed as:

$$MAE = \frac{1}{N}\sum_{i=1}^{N}|y_i - \hat{y_i}| \quad (8)$$

where y_i and $\hat{y_i}$ are the observed and simulated values at time step i, respectively, and N is the number of observations.

3.4.4. Nash–Sutcliffe Efficiency (NSE)

NSE is a normalised dimensionless statistic that benchmarks model residual variance against the variance of the observed discharge record [70,71]. A value of NSE = 1 signals

a perfect match between simulated and observed series, NSE = 0 implies that the model performs no better than the observed mean as a predictor, and negative values indicate that the mean observed discharge would yield smaller prediction errors than the model itself [66]. NSE is defined as:

$$NSE = 1 - \frac{\sum_{i=1}^{N}(y_i - \hat{y_i})^2}{\sum_{i=1}^{N}(y_i - \bar{y})^2} \quad (9)$$

where y_i is the observed value, ŷ□ is the simulated value, ȳ is the mean of all observed values, and N is the total number of observations.

3.5. Benchmark Models and Skill Score

Nash–Sutcliffe efficiency is referenced to the variance of the observed series rather than to an alternative forecast. For a one-step-ahead forecast of an hourly discharge series in a small, strongly autocorrelated catchment, a high NSE can therefore be obtained without any genuine forecasting skill, since the autocorrelation of the series alone explains most of its variance [72–74]. To separate the contribution of the Singh fuzzy scheme from the inherent predictability of the series, two benchmark predictors were evaluated for each event over the same forecast points and with the same metrics.

The first is the persistence, or naïve, forecast, which carries the last observation forward:

$$Q_{t+1} = Q_t \quad (10)$$

The second is a first-order autoregressive model fitted by ordinary least squares to the same event window from which the fuzzy partition is derived, so that both models draw on identical information:

$$Q_{t+1} = c + \varphi.Q_t \quad (11)$$

Forecast skill relative to the persistence benchmark was quantified using the skill score:

$$SS = 1 - \frac{MSE\ (model)}{MSE\ (persistance)} \quad (12)$$

where MSE denotes the mean squared error. SS = 1 indicates a perfect forecast, SS = 0 indicates performance identical to persistence and SS < 0 indicates that the naïve forecast would be preferable.

4. Results and Discussion

4.1. Time Series Temporal Resolution Conversion

Transitioning from 15 min to hourly discharge records yielded a more stable and better-conditioned input representation for the fuzzy framework, for the following reasons:

(a) Noise Reduction: Data aggregation reduced high-frequency noise and increased the signal-to-noise ratio, allowing underlying hydrological trends to be resolved more clearly.
(b) Temporal Dynamics: The hourly series better matched the temporal dynamics of the Singh fuzzification scheme, as smoother discharge transitions produced more representative difference-based forecasting parameters.
(c) Statistical: Statistically, hourly aggregation attenuated short-lag autocorrelation and reduced local variance, which stabilised membership function boundary estimation and led to more uniformly populated fuzzy intervals.
(d) Computational: The reduced data dimensionality also lowered computational overhead, making the fuzzification and ACF/PACF diagnostic steps more tractable.

A limitation of hourly aggregation is the potential loss of short-duration extreme peaks and fine-scale temporal variability, which may reduce the representation of rapidly evolving flood dynamics. However, under data-scarce conditions, the improved statistical stability and more reliable estimation of fuzzy membership functions were considered to outweigh this loss of temporal detail.

Collectively, these properties provided a more stable input representation for the proposed fuzzy-logic forecasting framework. Accordingly, these findings describe the effect of temporal aggregation on the statistical characteristics of the input data and the stability of the proposed fuzzy-logic framework.

4.2. Autocorrelation Function (ACF)

The ACF results for the four flood events are presented in Figure 4a–d. All events exhibit significant positive autocorrelations at lag 1, confirming the presence of short-term temporal persistence. However, the decay rates, persistence horizons, and correlation structures differ markedly across events, indicating heterogeneous and potentially nonlinear temporal dynamics. Event 1 displays the slowest decay. Significant positive autocorrelations persist beyond lag 48 before crossing into negative territory, suggesting prolonged hydrological memory. The gradual, non-exponential decline implies that antecedent discharge conditions influence the system response nonlinearly over an extended window. The persistence of significant coefficients across a wide lag range introduces uncertainty regarding the appropriate memory length for modelling. Event 2 exhibits a faster decay, with correlations dropping below the 95% confidence bounds near lag 24. The transition to non-significant values is comparatively abrupt, indicating a shorter but still meaningful hydrological memory. The asymmetric decay pattern suggests a nonlinear attenuation of antecedent influences. Event 3 follows a similar but slightly slower decay profile than Event 2. Correlations remain weakly significant up to approximately lag 26 before converging to zero. Minor oscillatory deviations around zero are observable at intermediate lags, implying the superposition of multiple temporal processes and adding complexity to the dependence structure. Event 4 presents the most complex ACF pattern. Alternating positive and negative correlations appear cyclically throughout the lag domain, producing a quasi-periodic oscillatory structure absent in the other events. This behaviour is indicative of multiple interacting hydrological mechanisms operating at different temporal scales. The oscillation introduces strong nonlinearity and structural uncertainty, as no single linear autoregressive model can replicate such a pattern.

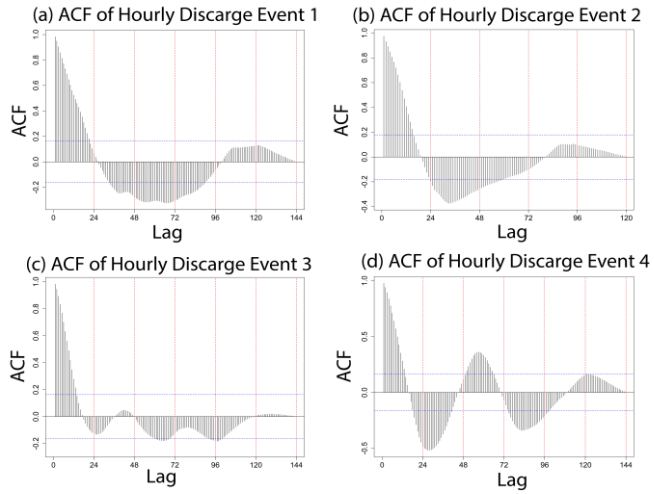


Figure 4. ACF plots of hourly discharge: (**a**) Event 1, (**b**) Event 2, (**c**) Event 3, and (**d**) Event 4.

Collectively, the four events reveal a complex temporal dependence structure that varies in persistence length, decay rate, and oscillatory character. The event-specific heterogeneity implies that the temporal dynamics are uncertain and cannot be represented by a unified linear dependence framework. These characteristics—(a) nonlinearity in decay, (b) uncertainty in memory length, and (c) complex multi-scale dependence—provide quantitative motivation for adopting the Singh fuzzy logic approach, which accommodates flexible, rule-based inference without imposing restrictive linearity assumptions.

4.3. Partial Autocorrelation Function (PACF)

The PACF results for the four flood events are presented in Figure 5a–d. For all events, a dominant spike at lag 1 confirms that the immediately preceding discharge observation is the primary direct predictor. Beyond lag 1, the PACF structures diverge considerably, revealing event-specific nonlinear and complex dependence patterns. For Event 1, partial autocorrelations remain near zero after lag 1 but display persistent low-amplitude fluctuations across the lag domain. These scattered deviations suggest weak secondary direct dependencies at multiple temporal scales. Their irregular distribution implies that the residual structure is not captured by a simple autoregressive model, introducing uncertainty in selecting an appropriate model order. Event 2 shows a similar overall structure, with the dominant lag-1 spike followed by several isolated significant peaks at intermediate lags. These localised spikes indicate direct higher-order dependencies that are event-specific and inconsistent across the lag range. Such irregularity is characteristic of nonlinear and uncertain temporal interactions. Event 3 exhibits a comparatively regular PACF after lag 1, with most coefficients remaining within the 95% confidence bounds. Nevertheless, small but consistent deviations persist throughout the lag domain. These deviations indicate that the process is not fully described by a first-order linear structure, providing evidence of residual nonlinearity. The persistence of these low-amplitude deviations across multiple lags further reflects complex temporal dependence at secondary scales. Moreover, the absence of a clearly dominant higher-lag structure introduces uncertainty regarding whether a purely autoregressive model of any fixed order could reliably capture the dependence pattern. Event 4 presents the most irregular PACF pattern. Alternating positive and negative partial autocorrelations appear at several lag positions beyond lag 1, mirroring the oscillatory behaviour observed in the ACF. This structure indicates the presence of multiple competing direct influences operating simultaneously. The irregular sign alternation is a clear indicator of nonlinearity and precludes representation by any single low-order linear model.

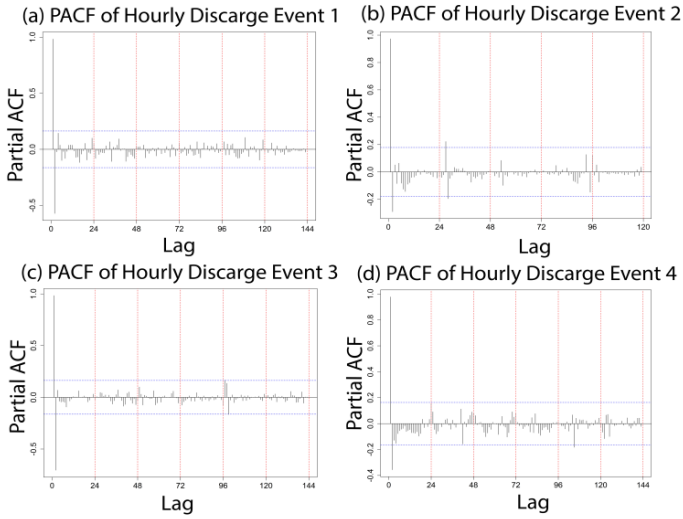


Figure 5. PACF plots of hourly discharge: (**a**) Event 1, (**b**) Event 2, (**c**) Event 3, and (**d**) Event 4.

Overall, the PACF results confirm that the discharge dynamics across all four events are governed by complex, heterogeneous, and time-varying direct dependencies. The dominant first-lag effect combined with event-specific higher-order interactions reflects a layered temporal structure that introduces both uncertainty in model specification and evidence of nonlinear behaviour. These findings reinforce the rationale for applying the Singh fuzzy logic framework, which handles uncertain and complex temporal dependencies through adaptive fuzzy rule-based inference rather than fixed linear parameterisation.

4.4. Fuzzification Using the Singh Method

To visualise the Singh fuzzification framework, the hourly discharge series of all four flood events was represented using eight fuzzy clusters (A1–A8) derived from the Singh partitioning concept. This representation enables continuous discharge variations to be interpreted as gradual transitions between neighbouring hydrological clusters. The resulting hydrograph partitioning and fuzzy-cluster transition matrix heatmaps are presented in Figures 6 and 7. For all events, transitions were predominantly concentrated near the main diagonal of the transition matrices, indicating that discharge evolution occurred mainly through neighbouring fuzzy clusters rather than abrupt jumps across distant clusters. This behaviour indicates that the fuzzy-cluster representation preserves the physical continuity of flood-wave propagation and avoids unrealistic transitions between distant hydrological clusters.

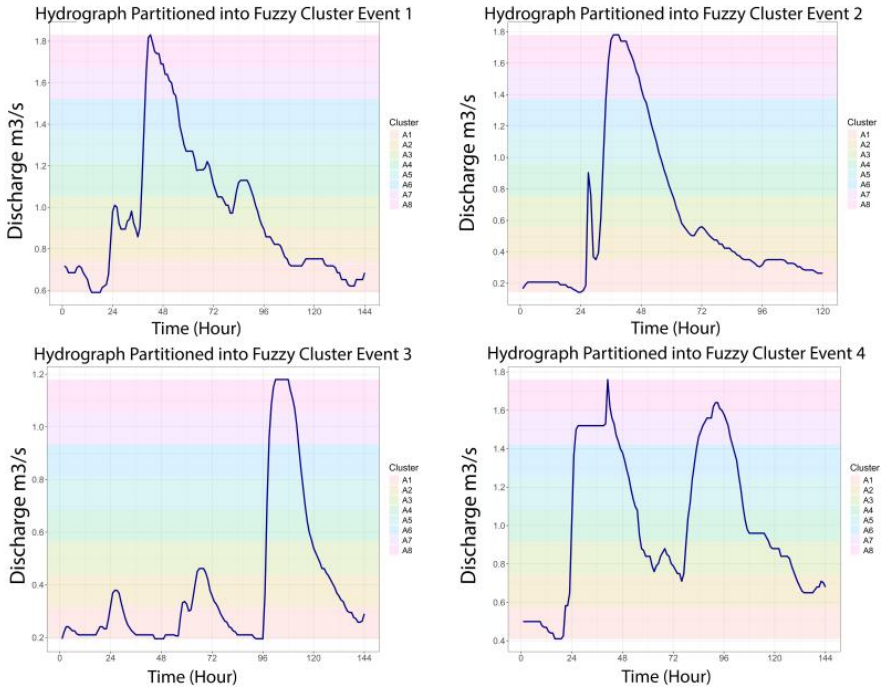


Figure 6. Singh-Based Fuzzy Cluster Partitioning of the Hourly Discharge Hydrograph.

First, Event 1 exhibited the broadest cluster occupancy, spanning almost the entire fuzzy domain from A1 to A8. The hydrograph shows a gradual rising limb followed by a prolonged recession phase, indicating sustained catchment storage release. This behaviour is reflected in the transition matrix, where strong self-transitions occur in lower and intermediate clusters, including A1→A1 = 0.96, A2→A2 = 0.81, A4→A4 = 0.78, and A5→A5 = 0.75. The upper clusters also reveal persistent transitions, particularly A8→A8 = 0.88. These high diagonal probabilities indicate strong temporal persistence and relatively smooth inter-cluster evolution, consistent with the long persistence previously observed in the ACF. By contrast, Event 2 displayed a rapid rise toward peak discharge followed by a mono-

tonic recession. Compared with Event 1, the hydrograph spent less time in high-discharge clusters, indicating a more impulsive flood response. The transition matrix confirms this behaviour through stronger localization in fewer clusters. Lower-cluster persistence remained high (A1→A1 = 0.96; A2→A2 = 0.88), while upper clusters showed concentrated transitions such as A6→A6 = 0.67 and A8→A8 = 0.91. The high probability of A7→A8 = 0.60 indicates a rapid escalation toward peak conditions. Statistically, this suggests reduced state dispersion and lower transition entropy compared with Event 1. Furthermore, Event 3 exhibited the most asymmetric hydrograph. Discharge remained in low clusters for an extended period before a sharp transition toward peak flow near hour 100. This delayed response is clearly reflected in the transition matrix. Strong persistence in lower clusters was observed (A1→A1 = 0.95; A2→A2 = 0.76; A3→A3 = 0.83), followed by abrupt transitions toward upper clusters during the flood peak. Particularly, A7→A8 = 0.50 and A8→A8 = 0.92 indicate strong peak persistence once extreme flow conditions were reached. Hydrologically, this pattern suggests threshold-driven runoff generation, where flow remains stable until a critical triggering condition is exceeded. Finally, Event 4 exhibited the most complex behaviour. Unlike the other events, the hydrograph shows two major peaks separated by a recession period, indicating multi-peak flood dynamics and multiple runoff-generation mechanisms. This complexity is reflected directly in the transition matrix. While lower-cluster persistence remained high (A1→A1 = 0.95; A2→A2 = 0.89; A3→A3 = 0.91), upper-cluster transitions were substantially more dispersed. Notably, A6→A6 = 0.64, A7→A7 = 0.87, and A8→A8 = 0.71 indicate weaker persistence at extreme flows compared with Events 1–3. The stronger off-diagonal transitions among upper clusters suggest repeated switching between high-flow states, consistent with the oscillatory behaviour previously identified in the ACF and PACF analyses.

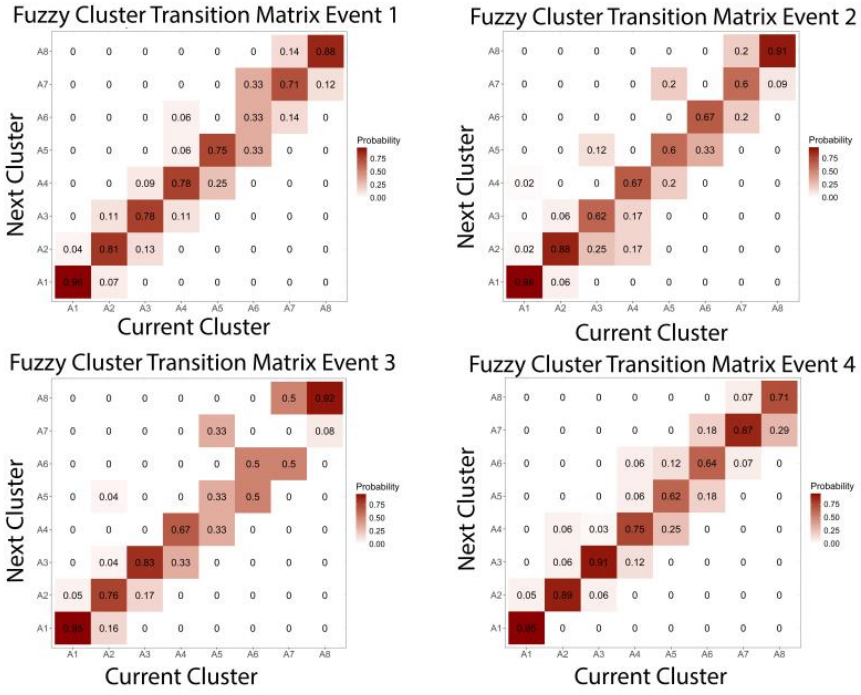


Figure 7. Heatmap of Fuzzy-Cluster Transition Probabilities.

Comparing all events, Event 1 showed the smoothest and most persistent fuzzy-cluster evolution, whereas Event 4 exhibited the highest transition complexity and strongest upper-cluster variability. Events 2 and 3 occupied intermediate positions, with Event 2 showing rapid but structured transitions and Event 3 demonstrating delayed threshold-driven escalation. Collectively, the hydrograph partitioning and transition matrices indicate that the

Singh-based fuzzy-cluster representation successfully captures both gradual and abrupt hydrological transitions while preserving the main temporal dependence structures of the discharge series. These findings further support the suitability of fuzzy logic for modelling nonlinear, uncertain, and complex discharge dynamics under short-term flood conditions.

4.5. Fuzzy Logic Modelling

The predictive performance of the Singh-based fuzzy logic model was evaluated using hydrograph comparison, prediction-error distribution, and observed–predicted scatter analysis, as presented in Figures 8–10. Overall, the model reproduced the discharge dynamics of all four flood events with close agreement, demonstrating that the fuzzy rule-based framework effectively captured both gradual and abrupt hydrological transitions across contrasting catchment responses. All performance metrics reported in this section refer to one-hour-ahead (one-step) forecasts of the hourly discharge series.

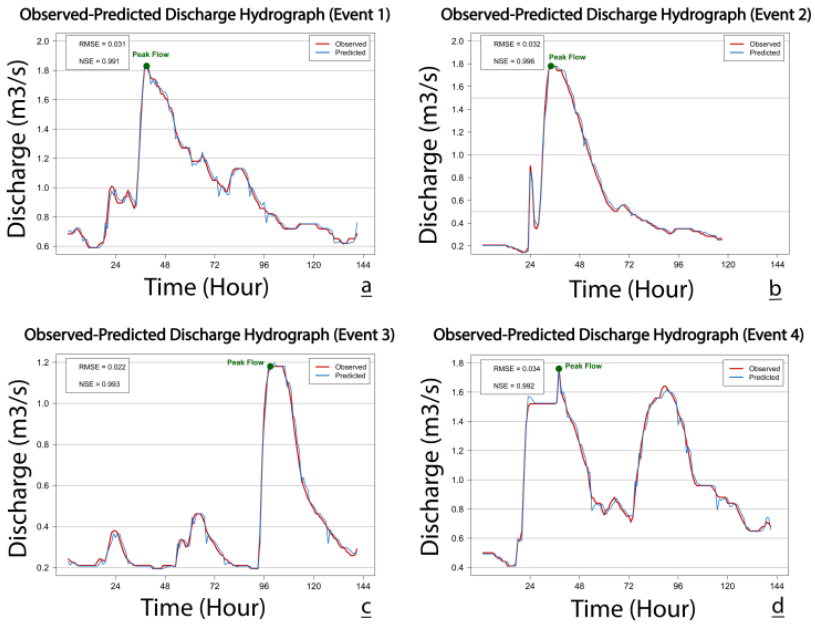


Figure 8. Observed vs. Predicted Discharge Values: (**a**) Event 1; (**b**) Event 2; (**c**) Event 3; (**d**) Event 4.

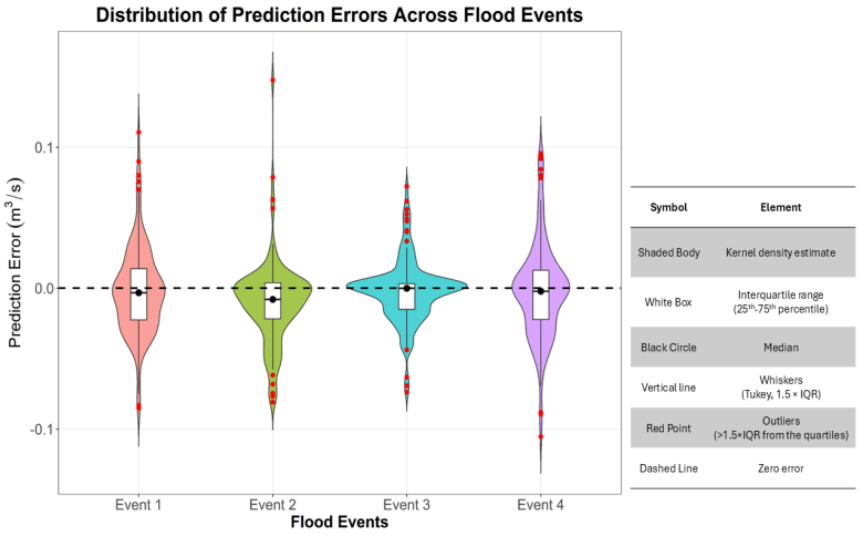


Figure 9. Violin Plot of Error Distribution for Events 1–4.

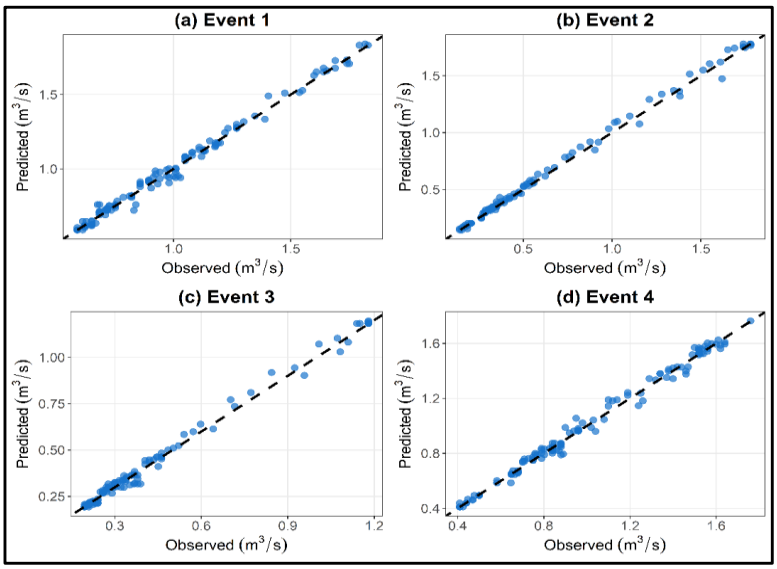


Figure 10. 1:1 Observed vs. Predicted Discharge Values: (**a**) Event 1; (**b**) Event 2; (**c**) Event 3; (**d**) Event 4.

In Event 1, the predicted hydrograph almost entirely overlaps the observed curve throughout the entire time series, including the rising limb, peak, and extended recession phase. A notable characteristic of this event is the oscillatory behaviour around the peak: unlike Events 2–4, where discharge drops sharply following the maximum, Event 1 shows repeated low-amplitude fluctuations both before and after the peak on the observed hydrograph, a pattern that the model reproduced with high fidelity (Figure 8). This persistent oscillatory structure, rather than a single clean recession, is consistent with the slowest ACF decay among all events and the strongest temporal autocorrelation, reflecting a gradual, memory-dominated catchment response. Because neighbouring fuzzy membership states evolve continuously under such conditions, the model transitions smoothly between rules, resulting in near-perfect tracking. This is confirmed by the dense clustering of points along the 1:1 line in Figure 10a and the narrowest violin distribution in Figure 9, with the median error closest to zero across all events. Event 2 delivers similarly strong performance, yet its hydrograph shape is structurally different: discharge rises steeply to a single, well-defined peak before declining rapidly, in contrast to the prolonged oscillatory tail of Event 1. Minor deviations appear near the peak and during the early recession, where the rate of decline is steepest, but these remain small relative to the overall discharge range. The faster ACF decay compared with Event 1 indicates shorter temporal memory, meaning antecedent discharge conditions lose predictive influence more quickly. Hydrologically, this implies a faster catchment response, likely reflecting lower initial soil moisture storage or higher drainage efficiency—which explains the slightly elevated uncertainty around peak formation. Figure 10b confirms limited dispersion around the 1:1 line, and the compact violin in Figure 9 shows a near-zero median error with only modest spread, indicating that the model captured the dominant runoff dynamics despite the quicker system response.

Event 3 presents a more distinctive hydrological signature: a gradual pre-peak discharge increase spanning several time steps before the main peak is reached, suggesting antecedent flow accumulation driven by prior rainfall inputs or slow subsurface drainage, a seasonal or multi-episode characteristic. The model reproduces the general shape well, including this pre-peak rising trend, but local mismatches increase near the abrupt final rise to peak and during the subsequent rapid transitions. Figure 10c shows a wider spread of points from the 1:1 line, particularly at higher discharge values, and Figure 9 displays a broader violin distribution compared with Events 1 and 2. The ACF and PACF analyses previously

indicated weaker overall persistence combined with localised higher-order dependencies, consistent with the superposition of slow subsurface contributions on faster surface runoff. This multi-mechanism character increases the complexity of fuzzy state transitions, making exact reproduction of sharp local changes more difficult. Event 4 is structurally the most complex, exhibiting two distinct discharge peaks of comparable magnitude rather than a single dominant peak—a double-peaked structure visible in Figure 8 that reflects sequential or interacting runoff-generation pulses. The model successfully captures the timing and approximate magnitude of both peaks and reconstructs the main hydrograph shape; however, larger deviations arise during the rapidly oscillating discharge phases between and around the two peaks. Figure 10d shows the widest scatter around the 1:1 line, concentrated at intermediate-to-high discharges where the oscillatory fluctuations are most pronounced. Figure 9 confirms the broadest violin distribution and the most pronounced outliers among all events. The oscillatory ACF structure and alternating PACF signs identified earlier indicate quasi-periodic behaviour driven by competing lag-specific influences, hydrologically consistent with alternating infiltration-dominated and runoff-dominated responses that interact across different temporal scales.

A cross-event comparison highlights a clear gradient of predictive performance linked to hydrological complexity. Events 1 and 2, despite their different recession shapes, share a relatively simple single-peak structure and strong temporal coherence, yielding near-overlapping predicted and observed hydrographs (Figure 8), tight 1:1 clustering (Figure 10), and narrow error distributions (Figure 9). Importantly, the model correctly identified the timing and magnitude of the single peak in both events, confirming that the fuzzy transition rules can resolve dominant discharge maxima when the hydrograph is governed by a coherent, memory-rich signal. Events 3 and 4 introduce additional complexity—pre-peak accumulation dynamics and a double-peaked structure, respectively—which widens prediction errors; nonetheless, the model successfully detected both peaks in Event 4 and reproduced the pre-peak rising trend in Event 3, with errors remaining symmetric around zero in both cases. This indicates that even under multi-mechanism or multi-pulse forcing, the framework avoids systematic bias and retains peak-detection capability, though local timing and magnitude accuracy inevitably decrease as temporal complexity increases. Collectively, Figures 8–10 confirm that predictive performance is governed primarily by the degree of nonlinearity and temporal structure inherent to each event rather than by model deficiencies. The event rainfall characteristics support this interpretation. Event 1 received the largest event precipitation total (58.0 mm) and produced the highest peak (1.83 m^3/s), whereas Event 3 received the smallest total (43.8 mm) and produced the lowest peak (1.18 m^3/s). However, Event 3 also recorded the highest maximum 10 min precipitation (19.5 mm). Accordingly, short-duration rainfall intensity alone did not govern peak magnitude. Event rainfall depth and antecedent catchment conditions appear to exert the stronger control, although antecedent soil moisture was not quantified in this study.

Table 3 demonstrates that the fuzzy logic model achieved consistently low forecast errors across all four events, with NSE values exceeding 0.99, indicating excellent agreement between observed and simulated discharge dynamics. Among the events, Event 2 showed the best overall performance (NSE = 0.996), suggesting that its hydrological response was captured most accurately, likely due to a more stable rainfall–runoff relationship and smoother discharge transitions. In contrast, Event 3 exhibited the highest MAPE (4.042%) despite the lowest RMSE (0.022 m^3/s), implying that percentage-based errors became more pronounced during lower discharge periods, where small absolute deviations translate into larger relative errors. Events 1 and 4 showed slightly higher RMSE and MAE values, which may reflect greater uncertainty during rapid rising or recession limbs of the hydrograph, where nonlinear runoff processes and short-term discharge fluctuations are more difficult to

model. Overall, these metrics complement the previous graphical analyses by quantifying the fit of the fuzzy logic model under varying hydrological conditions; these values are placed against benchmark predictors in Section 4.6.

Table 3. Evaluation metrics of the Singh fuzzy logic model and of the persistence and AR(1) benchmarks for Events 1–4, with the skill score (SS) relative to persistence.

Event	Model	RMSE (m^3/s)	MAPE (%)	MAE (m^3/s)	NSE	SS
Event 1	Singh Fuzzy	0.031	2.478	0.023	0.991	0.612
	Persistence	0.050	2.448	0.026	0.976	-
	AR(1)	0.050	2.544	0.026	0.977	0.005
Event 2	Singh Fuzzy	0.032	3.744	0.021	0.996	0.897
	Persistence	0.100	5.670	0.038	0.958	-
	AR(1)	0.099	6.911	0.041	0.958	0.012
Event 3	Singh Fuzzy	0.022	4.042	0.015	0.993	0.777
	Persistence	0.047	4.670	0.021	0.972	-
	AR(1)	0.046	5.285	0.022	0.972	0.009
Event 4	Singh Fuzzy	0.034	2.528	0.025	0.992	0.714
	Persistence	0.064	3.195	0.033	0.973	-
	AR(1)	0.063	3.611	0.036	0.974	0.011

SS: Skill Score relative to persistence. Fitted AR(1) coefficients (c, φ): Event 1 (0.011, 0.989); Event 2 (0.014, 0.977); Event 3 (0.007, 0.985); Event 4 (0.019, 0.983). Benchmark metrics are computed over the $N - 1$ forecast pairs of each event window; NSE denominators use the variance of the full event series.

4.6. Benchmark Comparison and Forecast Skill

Table 3 additionally reports the two benchmark predictors and the skill score of the fuzzy model relative to persistence. As anticipated, the persistence forecast alone achieves NSE between 0.958 (Event 2) and 0.976 (Event 1). This confirms that at a one-hour lead time on hourly discharge in a 135 km^2 catchment, a large fraction of the observed variance is explained by the autocorrelation of the series itself, and that NSE values above 0.99 must therefore be interpreted against this baseline rather than in absolute terms. The AR(1) benchmark performs essentially identically to persistence, with skill scores of 0.005–0.012, consistent with the fitted coefficients lying close to unity ($\varphi = 0.977$–0.989); a linear first-order structure thus adds nothing beyond carrying the last observation forward.

Against this baseline, the Singh fuzzy framework retains a clear advantage. RMSE is reduced by 38% for Event 1, 68% for Event 2, 53% for Event 3 and 47% for Event 4, corresponding to skill scores of 0.612, 0.897, 0.777 and 0.714, respectively. The largest gain occurs for Event 2, the event with the steepest rise and fastest recession, where a persistence forecast systematically lags the hydrograph; the smallest gain occurs for Event 1, whose slow, memory-dominated evolution is already well approximated by the preceding observation. This ordering indicates that the fuzzy rule base contributes most where discharge changes fastest, that is, precisely in the situations that matter for flood early warning. It should be noted that for Event 1, the persistence MAPE (2.448%) is marginally lower than that of the fuzzy model (2.478%), so for that event, the improvement is confined to the squared- and absolute-error metrics, which weight the rapidly changing limbs of the hydrograph more heavily.

5. Conclusions

Short-term discharge forecasting is critical for flood resilience, yet conventional ML- and DL-based models struggle under data-scarce and highly variable hydrological conditions [75,76]. To address this, the present study proposes a Singh fuzzy logic framework for transparent, interpretable, and computationally efficient discharge and flood peak prediction. This study applies the Singh fuzzy partitioning scheme to four events of hourly discharge time series from the Schwarzbach catchment. Membership functions cluster discharge data according to statistical behaviour, enabling predictions drawn from both local and neighbouring discharge states. ACF, PACF, and cluster transition analysis link each event's temporal structure to model performance, explaining why accuracy varies across events.

Three principal findings emerged: (a) Hourly temporal aggregation improved fuzzy membership stability by reducing high-frequency noise and stabilising local variance. This confirms that temporal preprocessing is a critical step in fuzzy-based hydrological forecasting. (b) The ACF and PACF analyses revealed strong event-specific heterogeneity. All four events exhibited significant first-lag dependence. However, they differed markedly in persistence length and dependency structure: from the memory-dominated autocorrelation of Event 1 (CV = 0.337) to the oscillatory structure of Event 4 (CV = 0.383). This demonstrates that Schwarzbach discharge dynamics reflect nonlinear, time-varying hydrological controls. (c) Benchmarked against a persistence forecast, the Singh fuzzy framework reduced RMSE by 38–68%, corresponding to skill scores of 0.612–0.897, while reproducing all four flood events with NSE exceeding 0.99 and correctly identifying peak timing and magnitude, including the double-peaked structure of Event 4. Prediction uncertainty scaled with event-specific hydrological complexity rather than with systematic model bias.

All four events achieved NSE $\geq$ 0.991. Because NSE is referenced to the variance of the observed record rather than to an alternative forecast, these values were benchmarked against a persistence predictor, which itself attains NSE between 0.958 and 0.976 for the same events; an AR(1) benchmark adds essentially nothing to persistence. Relative to persistence, the fuzzy framework reduces RMSE by 38–68%, corresponding to skill scores of 0.612–0.897. The improvement is therefore substantive, but it is reported in these terms rather than through the absolute NSE alone. Event 2 delivered the highest skill score (SS = 0.897), reflecting a steep single-peak hydrograph that a naïve forecast systematically lags, while Event 1 delivered the lowest (SS = 0.612), consistent with its slow, memory-dominated evolution being already well described by the preceding observation. Event 3 recorded the lowest RMSE (0.022 m^3/s) but the highest MAPE (4.042%), driven by low base-flow values amplifying relative errors, and Event 4 maintained SS = 0.714 despite its double-peaked complexity. These results are consistent with prior studies confirming that fuzzy logic models handle nonlinear hydrological boundaries without imposing restrictive statistical assumptions [75,77]. Multi-mechanism and threshold-controlled events are known to produce higher prediction uncertainty across model types [77,78]. In contrast to black-box approaches such as deep learning methods, which require large training datasets and offer limited mechanistic transparency [76], the proposed framework attains this level of skill from short-term time series of 5–6 days while retaining a fully inspectable rule base. Taken together with the correct reproduction of peak timing and magnitude, including the double-peak structure of Event 4, it is this combination of a measurable improvement over a naïve benchmark and full interpretability, rather than the absolute NSE value, that constitutes the practical contribution of the framework in data-scarce operational contexts.

The framework is particularly suited to (i) flood early warning systems in catchments with limited data and highly variable storm-driven responses; (ii) decision-support tools for water authorities requiring transparent rule-based outputs; and (iii) hydrological re-

search in underrepresented regions where interpretable models yield both predictive and scientific value.

Five limitations should be noted. First, calibration on four events from a single catchment constrains transferability of the fuzzy membership boundaries to other hydrological regimes or climatic settings without re-calibration. Second, the discharge-only predictor structure cannot encode the multi-mechanism forcing—pre-peak accumulation in Event 3 and double-pulse dynamics in Event 4—that drove the largest prediction errors, as antecedent rainfall intensity and soil moisture state remain unrepresented. Third, the framework is restricted to a one-hour-ahead forecasting horizon; longer lead times of several hours to days, which are frequently required in operational early warning practice, were not evaluated and would be expected to exhibit progressively reduced forecasting skill. Fourth, data scarcity was emulated by restricting the model to event-scale subsets of a well-monitored record, rather than encountered in the field. Accordingly, transferability to genuinely ungauged or sparsely monitored catchments remains to be tested. Fifth, the universe of discourse and the interval length are derived from the complete event window and therefore presuppose knowledge of the event maximum. Although these are not fitted parameters, this configuration cannot be reproduced in real time, and the sensitivity of the interval length to the portion of the event used for its estimation, quantified in Section 3.3, indicates that an a priori or recursively updated definition of U and L is a prerequisite for operational deployment.

Future work should therefore (i) incorporate rainfall intensity and antecedent soil moisture as additional fuzzy input variables to extend the framework toward a coupled hydrometeorological forecasting system; (ii) evaluate transferability across catchments of differing size, geology, and land cover to establish whether event-specific ACF diagnostics can serve as a pre-deployment suitability screening tool for operational early warning applications; (iii) extend the framework to longer forecasting horizons through recursive and direct multi-step formulations, and quantify how predictive skill degrades as the lead time increases from one hour to several hours or days; (iv) apply the framework in genuinely ungauged or sparsely monitored catchments, where data scarcity is encountered rather than emulated; (v) integrate synthetic mean hydrograph descriptors—total duration (T_t), time to peak (T_p) and shape coefficient (γ)—into the definition of the membership functions and the rule base, so that fuzzy rules can be conditioned on flood typology rather than on event-specific discharge magnitudes alone [79] (such a typology-based formulation would introduce regionalised information on average flood shape and could subsequently be tested against both additional observed events and theoretically generated single-peak and bimodal hydrographs); and (vi) fix U and L from an independent historical period of the same gauge, or update them recursively during the event, and quantify the resulting change in skill, thereby establishing the operationally attainable performance of the framework.

Concluding, this study demonstrates that interpretable fuzzy frameworks can bridge the gap between physical understanding and operational forecasting in data-limited flood-prone catchments.

Author Contributions: All authors contributed to the study conception and design. Conceptualization, methodology, software, validation, formal analysis, resources, data curation, writing—original draft preparation, visualisation, M.K. Investigation, writing—review and editing, M.K. and B.S. Supervision, project administration, funding acquisition, B.S. All authors have read and agreed to the published version of the manuscript.

Funding: This work has been funded by the LOEWE initiative (Hesse, Germany) within the emergenCITY centre [LOEWE/1/12/519/03/05.001(0016)/72].

Data Availability Statement: The hourly discharge series analysed in this study were derived from the 15 min record of the Nauheim gauge (ID 23980353), which is publicly accessible through the HLNUG data portal at https://www.hlnug.de/static/pegel/wiskiweb3/webpublic/#/overview/Durchfluss/station/41361/Nauheim/ (accessed on 5 February 2026) [30]. The 10 min precipitation observations of DWD station Frankfurt/Main Flughafen (ID 1420) are publicly available through the DWD Climate Data Center portal at https://cdc.dwd.de/portal/ (accessed on 5 February 2026) [31]. The extracted event windows and the derived model outputs are available from the corresponding author upon reasonable request.

Acknowledgments: We would like to especially thank the Hessian Agency for Nature Conservation, Environment, and Geology (HLNUG) and the German Weather Service (DWD) for providing data.

Conflicts of Interest: The authors have no relevant financial or non-financial interests to disclose.

References

1. CRED; UNDRR. *Human Cost of Disasters: An Overview of the Last 20 Years: 2000–2019*; CRED/UNDRR: Geneva, Switzerland, 2020.
2. Khazaeiathar, M.; Schmalz, B. Addressing volatility and nonlinearity in discharge modeling: ARIMA-iGARCH for short-term hydrological time series simulation. *Hydrology* **2025**, *12*, 197. [CrossRef]
3. Asif, M. Review and intercomparison of machine learning applications for short-term flood forecasting. *Water Resour. Manag.* **2025**, *39*, 1971–1991. [CrossRef]
4. Yeh, G.; Cheng, H.-P.; Cheng, J.-R.C.; Lin, H.-C.J.; Martin, W.D. *A Numerical Model Simulating Water Flow and Contaminant and Sediment Transport in Watershed Systems (WASH123D: Version 1.0)*; Technical Report CHL-98-19; US Army Corps of Engineers, Waterways Experiment Station: Vicksburg, MS, USA, 1998.
5. Feldman, A.D. *Hydrologic Modeling System HEC-HMS: Technical Reference Manual*; US Army Corps of Engineers, Hydrologic Engineering Center: Davis, CA, USA, 2000.
6. Rossman, L.A. *Storm Water Management Model User's Manual, Version 5.0*; US Environmental Protection Agency: Cincinnati, OH, USA, 2010.
7. Arnold, J.G.; Srinivasan, R.; Muttiah, R.S.; Williams, J.R. Large area hydrologic modeling and assessment part I: Model development. *J. Am. Water Resour. Assoc.* **1998**, *34*, 73–89. [CrossRef]
8. Bheeman, P.; Rangarajan, S. Impact of climate change on the upper Bhavani watershed using SWAT model. *Results Eng.* **2025**, *27*, 105905. [CrossRef]
9. Yousif, Y.T.; Hamdan, A.N.A. Flood simulation utilizing HEC-HMS and HEC-RAS. *Civ. Eng. J.* **2026**, *12*, 231–251. [CrossRef]
10. Mahmoodi, E.; Azari, M.; Dastorani, M.T.; Salvati, A. Comparison of hydrological modeling, artificial neural networks and multi-criteria decision-making approaches for determining flood source areas. *Water Resour. Manag.* **2024**, *38*, 5343–5363. [CrossRef]
11. Kumar, V.; Sharma, K.V.; Caloiero, T.; Mehta, D.J.; Singh, K. Comprehensive overview of flood modeling approaches: A review of recent advances. *Hydrology* **2023**, *10*, 141. [CrossRef]
12. Sîrbu, N.; Rugină, A.-M. Short-term streamflow forecasting for river management, using ARIMA models and recurrent neural networks. *Hydrology* **2026**, *13*, 82. [CrossRef]
13. Yavuz, V.S. Forecasting monthly rainfall and temperature patterns in Van Province, Türkiye, using ARIMA and SARIMA models: A long-term climate analysis. *J. Water Clim. Change* **2025**, *16*, 800. [CrossRef]
14. Ayiah-Mensah, F.; Bosson-Amedenu, S.; Mensah Baah, E.; Awuah Addor, J. Advancements in seasonal rainfall forecasting: A seasonal auto-regressive integrated moving average model with outlier adjustments for Ghana's Western Region. *Sci. Afr.* **2025**, *26*, e02632. [CrossRef]
15. Wu, X.; Zhao, Y.; Zhang, W.; Li, X.; Qin, G.; Li, H. Probabilistic early warning of flash floods using Monte Carlo simulation and hydrological modeling. *Eng. Appl. Comput. Fluid Mech.* **2025**, *19*, 2523423. [CrossRef]
16. Bhatt, P.; Sethi, A.; Tasgaonkar, V.; Shroff, J.; Pendharkar, I.; Desai, A.; Sinha, P.; Deshpande, A.; Joshi, G.; Rahate, A.; et al. Machine learning for cognitive behavioral analysis: Datasets, methods, paradigms, and research directions. *Brain Inform.* **2023**, *10*, 13. [CrossRef] [PubMed]
17. Yaaqob, K.Y.; Sadiq, S.S. Hybrid deep learning flood forecasting framework optimized with the snake algorithm. *Stat. Optim. Inf. Comput.* **2026**, *15*, 4114–4137. [CrossRef]
18. Deulkar, A.M.; Dixit, P.R.; Londhe, S.N.; Jain, R.K. Comparative assessment of artificial neural networks (ANNs), long short term memory network (LSTM) and HEC-HMS for runoff modeling. *Water Resour. Manag.* **2025**, *39*, 2049–2068. [CrossRef]
19. Zhou, F.; Chen, Y.; Liu, J. Application of a new hybrid deep learning model that considers temporal and feature dependencies in rainfall–runoff simulation. *Remote Sens.* **2023**, *15*, 1395. [CrossRef]

20. Manoli, B.; Poudel, S.; Koval, D.K.; Murphy, S.Y.; Steinschneider, S.; Lamontagne, J. Deep learning error post-processing improves stochastic watershed modeling. *J. Hydrol.* **2026**, *675*, 135663. [CrossRef]
21. Mamalakis, A.; Ebert-Uphoff, I.; Barnes, E.A. Explainable artificial intelligence in meteorology and climate science: Model fine-tuning, calibrating trust and learning new science. In *Extending Explainable AI Beyond Deep Models and Classifiers*; Springer: Berlin/Heidelberg, Germany, 2020; pp. 315–339.
22. Zhu, F.; Zhu, O.; Han, M.; Liu, W.; Guo, X.; Hou, T.; Zhao, L.; Xu, C.; Zhong, P. A hybrid process-data driven framework for real-time hydrological forecasting with interpretable deep learning. *J. Hydrol.* **2025**, *662*, 134082. [CrossRef]
23. Ampas, H.; Refanidis, I.; Ampas, V. Hybrid hydrological forecasting through a physical model and a weather-informed transformer model: A case study in Greek watershed. *Appl. Sci.* **2025**, *15*, 6679. [CrossRef]
24. Chen, J.; Guo, J.; Gu, J.; Zhang, K. Streamflow simulation and interpretability analysis in multi-climatic basins using physics-based and data-driven hybrid models. *Water Resour. Manag.* **2026**, *40*, 244. [CrossRef]
25. Zhang, C.; Li, H.; Hu, Y.; Shen, D.; Xu, B.; Chen, M.; Chu, W.; Li, R. A differentiability-based processes and parameters learning hydrologic model for advancing runoff prediction and process understanding. *J. Hydrol.* **2025**, *661*, 133594. [CrossRef]
26. Alvisi, S.; Mascellani, G.; Franchini, M.; Bárdossy, A. Water level forecasting through fuzzy logic and artificial neural network approaches. *Hydrol. Earth Syst. Sci.* **2006**, *10*, 1–17. [CrossRef]
27. Wee, G.; Chang, L.; Chang, F.; Amin, M.Z.M. A flood impact-based forecasting system by fuzzy inference techniques. *J. Hydrol.* **2023**, *625*, 130117. [CrossRef]
28. HLNUG. *Nauheim Gauge (ID23980353) in Hesse, Germany: Station Information*; Hessian Agency for Nature Conservation, Environment and Geology: Wiesbaden, Germany, 2023. Available online: https://www.hlnug.de/static/pegel/wiskiweb3/webpublic/#/overview/Durchfluss/station/41361/Nauheim/stationInfoHlnug (accessed on 13 May 2025).
29. LUBW. *Deutsches Gewässerkundliches Jahrbuch DGJ, Rheingebiet Teil I 2009*; Landesanstalt für Umwelt, Messungen und Naturschutz Baden-Württemberg: Karlsruhe, Germany, 2011. Available online: https://pd.lubw.de/38631 (accessed on 13 March 2024).
30. HLNUG. *Nauheim Gauge (ID23980353) in Hesse, Germany: Discharge Data [Data Set]*; Hessian Agency for Nature Conservation, Environment and Geology: Wiesbaden, Germany, 2023. Available online: https://www.hlnug.de/static/pegel/wiskiweb3/webpublic/#/overview/Durchfluss/station/41361/Nauheim/ (accessed on 5 February 2026).
31. DWD. *Precipitation Data from Station Frankfurt/M. (Flughfn.) ID 1420 [Data Set]*; Germany's National Meteorological Service (Deutscher Wetterdienst): Offenbach, Germany, 2023. Available online: https://cdc.dwd.de/portal/ (accessed on 5 February 2026).
32. Neal, C.; Reynolds, B.; Rowland, P.; Norris, D.; Kirchner, J.W.; Neal, M.; Sleep, D.; Lawlor, A.; Woods, C.; Thacker, S.; et al. High-frequency water quality time series in precipitation and streamflow: From fragmentary signals to scientific challenge. *Sci. Total Environ.* **2012**, *434*, 3–12. [CrossRef] [PubMed]
33. Zadeh, L.A. Fuzzy sets. *Inf. Control* **1965**, *8*, 338–353. [CrossRef]
34. Özelkan, E.C.; Duckstein, L. Fuzzy conceptual rainfall–runoff models. *J. Hydrol.* **2001**, *253*, 41–68. [CrossRef]
35. Nayak, P.C.; Sudheer, K.P.; Ramasastri, K.S. Fuzzy computing based rainfall–runoff model for real time flood forecasting. *Hydrol. Process.* **2005**, *19*, 955–968. [CrossRef]
36. Hassani, H.; Yarmohammadi, M.; Marvian Mashhad, L. Uncovering hidden insights with long-memory process detection: An in-depth overview. *Risks* **2023**, *11*, 113. [CrossRef]
37. Peiris, S.; Hunt, R. Revisiting the autocorrelation of long memory time series models. *Mathematics* **2023**, *11*, 817. [CrossRef]
38. Hyndman, R.J.; Athanasopoulos, G. *Forecasting: Principles and Practice*, 3rd ed.; OTexts: Melbourne, Australia, 2021; Available online: https://otexts.com/fpp3/ (accessed on 16 March 2025).
39. Danandeh Mehr, A.; Gandomi, A.H. A new evolutionary time series model for streamflow forecasting in boreal lake-river systems. *Theor. Appl. Climatol.* **2022**, *148*, 255–268. [CrossRef]
40. Hashemi, M.; Zamani, F.; Akhavan-Tabatabaei, R. Detrended fluctuation analysis of functional time series. *Physica A* **2024**, *653*, 130105. [CrossRef]
41. Guo, Y.; Li, J.; Zeng, H.; Zhang, T.; Feng, P.; Geng, J. Nonstationary flood frequency analysis using reconstructing past millennium floods based on large-scale climate indices. *J. Flood Risk Manag.* **2026**, *19*, e70189. [CrossRef]
42. Anderson, B.J.; Slater, L.J.; Rapson, J.; Brunner, M.I.; Dadson, S.J.; Yin, J.; Buechel, M. Stationarity assumptions in streamflow sensitivity to precipitation may bias future projections. *Earth's Future* **2025**, *13*, e2025EF006188. [CrossRef]
43. Wang, Y.; Zhang, X.; Zhao, K.; Singh, D. Stationarity of high- and low-flows under climate change and human interventions across global catchments. *Earth Space Sci.* **2024**, *11*, e2023EA003456. [CrossRef]
44. Wang, M.; Jiang, S.; Ren, J.; Yuan, S. A novel time-varying threshold level method for evaluating non-stationary hydrological drought. *J. Hydrol.* **2025**, *662*, 133977. [CrossRef]
45. Hassani, H.; Yeganegi, M.R. Unraveling time series dynamics: Evaluating partial autocorrelation function distribution and its implications. *Math. Comput. Appl.* **2024**, *29*, 58. [CrossRef]

46. Meng, X.; Zhang, J.; Zhao, J.; Wei, Z.; Ma, G. Monthly streamflow prediction of the source region of the Yellow River based on long short-term memory considering different lagged months. *Water* **2024**, *16*, 593. [CrossRef]
47. Gil-Alana, L.A.; Gupta, R.; Sauci, L.; Carmona-González, N. Temperature and precipitation in the US states: Long memory, persistence, and time trend. *Theor. Appl. Climatol.* **2022**, *150*, 1731–1744. [CrossRef] [PubMed]
48. Shumway, R.H.; Stoffer, D.S. *Time Series Analysis and Its Applications: With R Examples*, 4th ed.; Springer: New York, NY, USA, 2017. [CrossRef]
49. Box, G.E.P.; Jenkins, G.M.; Reinsel, G.C.; Ljung, G.M. *Time Series Analysis: Forecasting and Control*, 5th ed.; Wiley: Hoboken, NJ, USA, 2015. [CrossRef]
50. Singh, H.; Najafi, M.R.; Cannon, A.J. Understanding non-stationarity patterns in basin-scale hydroclimatic extremes. *Int. J. Climatol.* **2024**, *44*, 3867–3887. [CrossRef]
51. Papacharalampous, G.; Tyralis, H. A review of machine learning concepts and methods for addressing challenges in probabilistic hydrological post-processing and forecasting. *Front. Water* **2022**, *4*, 961954. [CrossRef]
52. Khan, M.M.H.; Muhammad, N.S.; El-Shafie, A. Wavelet based hybrid ANN-ARIMA models for meteorological drought forecasting. *J. Hydrol.* **2020**, *590*, 125380. [CrossRef]
53. Song, Q.; Chissom, B.S. Fuzzy time series and its models. *Fuzzy Sets Syst.* **1993**, *54*, 269–277. [CrossRef]
54. Chen, S.-M. Forecasting enrollments based on fuzzy time series. *Fuzzy Sets Syst.* **1996**, *81*, 311–319. [CrossRef]
55. Singh, S.R. A simple method of forecasting based on fuzzy time series. *Appl. Math. Comput.* **2007**, *186*, 330–339. [CrossRef]
56. Xian, S.; Zhang, J.; Xiao, Y.; Pang, J. A novel fuzzy time series model based on improved sparrow search algorithm and Pythagorean fuzzy set. *Soft Comput.* **2022**, *26*, 3653–3673.
57. Ramadhani, F.; Zarlis, M.; Suwilo, S. Fuzzy time series for short-term residential load forecasting in smart grids. *Sci. Rep.* **2025**, *15*, 34062. [CrossRef] [PubMed]
58. Nayak, P.C.; Sudheer, K.P.; Rangan, D.M.; Ramasastri, K.S. Short-term flood forecasting with a neurofuzzy model. *Water Resour. Res.* **2005**, *41*, W04004. [CrossRef]
59. Jahanbani, H.; Ahmed, A.N.; Bozorg-Haddad, O. Data-driven artificial intelligence-based streamflow forecasting: A review of methods, applications, and tools. *J. Am. Water Resour. Assoc.* **2024**, *60*, 1095–1119. [CrossRef]
60. Singh, S.R. A computational method of forecasting based on fuzzy time series. *Math. Comput. Simul.* **2008**, *79*, 539–554. [CrossRef]
61. Gautam, S.S.; Singh, S.R. Integrate new cross association fuzzy logical relationships to multi-factor high-order forecasting model of time series. *Int. J. Mach. Learn. Cybern.* **2021**, *12*, 2903–2919. [CrossRef]
62. Huarng, K. Effective lengths of intervals to improve forecasting in fuzzy time series. *Fuzzy Sets Syst.* **2001**, *123*, 387–394. [CrossRef]
63. Khalil, A.A.; Mandour, M.A.; Ali, A. The benefits of social insurance system prediction using a hybrid fuzzy time series method. *PeerJ Comput. Sci.* **2024**, *10*, e2500. [CrossRef] [PubMed]
64. Alyousifi, Y.; Othman, M.; Almohammedi, A.A. A novel stochastic fuzzy time series forecasting model based on a new partition method. *IEEE Access* **2021**, *9*, 80236–80252. [CrossRef]
65. Hodson, T.O. Root mean square error (RMSE) or mean absolute error (MAE): When to use them or not. *Geosci. Model Dev. Discuss.* **2022**, *15*, 5481–5487. [CrossRef]
66. Kim, S.; Kim, H. A new metric of absolute percentage error for intermittent demand forecasts. *Int. J. Forecast.* **2016**, *32*, 669–679. [CrossRef]
67. Hyndman, R.J.; Koehler, A.B. Another look at measures of forecast accuracy. *Int. J. Forecast.* **2006**, *22*, 679–688. [CrossRef]
68. Willmott, C.J.; Matsuura, K. Advantages of the mean absolute error (MAE) over the root mean square error (RMSE) in assessing average model performance. *Clim. Res.* **2005**, *30*, 79–82. [CrossRef]
69. Chai, T.; Draxler, R.R. Root mean square error (RMSE) or mean absolute error (MAE)? Arguments against avoiding RMSE in the literature. *Geosci. Model Dev.* **2014**, *7*, 1247–1250. [CrossRef]
70. Nash, J.E.; Sutcliffe, J.V. River flow forecasting through conceptual models part I—A discussion of principles. *J. Hydrol.* **1970**, *10*, 282–290. [CrossRef]
71. Moriasi, D.N.; Arnold, J.G.; Van Liew, M.W.; Bingner, R.L.; Harmel, R.D.; Veith, T.L. Model evaluation guidelines for systematic quantification of accuracy in watershed simulations. *Trans. ASABE* **2007**, *50*, 885–900. [CrossRef]
72. Seibert, J. On the need for benchmarks in hydrological modelling. *Hydrol. Process.* **2001**, *15*, 1063–1064. [CrossRef]
73. Schaefli, B.; Gupta, H.V. Do Nash values have value? *Hydrol. Process.* **2007**, *21*, 2075–2080. [CrossRef]
74. Knoben, W.J.M.; Freer, J.E.; Woods, R.A. Technical note: Inherent benchmark or not? Comparing Nash–Sutcliffe and Kling–Gupta efficiency scores. *Hydrol. Earth Syst. Sci.* **2019**, *23*, 4323–4331. [CrossRef]
75. Karami, M.; Shabanlou, S.; Mazaheri, H.; Mokhtari, S.; Najarchi, M. Integration of the non-linear time series GARCH model with fuzzy model optimized with water cycle algorithm for river streamflow forecasting. *Int. J. Comput. Intell. Syst.* **2024**, *17*, 156. [CrossRef]
76. Hadi, F.A.A.; Mohd Sidek, L.; Ahmed Salih, G.H.; Basri, H.; Sammen, S.S.; Mohd Dom, N.; Muhamad Ali, Z.; Najah Ahmed, A. Machine learning techniques for flood forecasting. *J. Hydroinform.* **2024**, *26*, 779–799. [CrossRef]

77. Tabbussum, R.; Dar, A.Q. Performance evaluation of artificial intelligence paradigms—Artificial neural networks, fuzzy logic, and adaptive neuro-fuzzy inference system for flood prediction. *Environ. Sci. Pollut. Res.* **2021**, *28*, 25265–25282. [CrossRef] [PubMed]
78. Heidari, L.; Khan, A.A. Probabilistic sub-daily streamflow forecasting in data-scarce catchments through a zero-shot inductive transfer learning approach. *J. Am. Water Resour. Assoc.* **2026**, *62*, e70115. [CrossRef]
79. Ilinca, C.; Albert, C.; Rozputniak, D.; Minghiraș, V. A novel approach to design flood hydrograph plotting in water management. *Appl. Sci.* **2026**, *16*, 4475. [CrossRef]

Disclaimer/Publisher's Note: The statements, opinions and data contained in all publications are solely those of the individual author(s) and contributor(s) and not of MDPI and/or the editor(s). MDPI and/or the editor(s) disclaim responsibility for any injury to people or property resulting from any ideas, methods, instructions or products referred to in the content.